Clays Clay Miner. (2023) 71:745–759
https://doi.org/10.1007/s42860-023-00266-0

ORIGINAL PAPER

Super-efficient Reduction of 4-nitrophenol Using Raw Pelagic Clays as Catalysts

Peiping Zhang · Tongtong Liu · Xue Sun · Qing Liang · Wei Zhang · Weikun Ning · Wenqing Li · Xuefa Shi · Shiding Miao

Accepted: 28 November 2023 / Published online: 26 December 2023

Abstract Natural clays are often employed as substrates for heterogeneous catalysts. However, the direct use of raw clays as catalysts has received less research attention. The objective of the present study was to help fill this gap by investigating catalytic properties of raw pelagic clays (PC) collected from the Indian Ocean. The raw PC were discovered to be efficient catalysts in the reduction of 4-nitrophenol (4-NP) in the presence of $NaBH_4$. The effects of parameters including pH values, dosages of PC, and initial concentration of 4-NP and $NaBH_4$ on the conversion or degradation rate of 4-NP have been investigated. The 4-NP was observed to be completely degraded within 480 s under conditions of 0.10 mM 4-NP, 25.0 mM $NaBH_4$, and 0.20 g/L PC at an initial pH value of 7.0. The apparent rate constant was evaluated to be 27.53×10^{-3} s^{-1}. Unlike previous pseudo-first order kinetics experiments, the induction period and degradation stages were observed to occur simultaneously during the PC catalysis. The S-shaped kinetics for 4-NP conversion was found to be perfectly matched by Fermi's function, and the enzyme-like catalysis by PC was appointed to describe the kinetics. Species of Fe(III), Mn(IV), and Mn(III) in PC were found to be essential, and were partly reduced to Fe(0) and Mn(II) by $NaBH_4$ in our reaction, contributing to rapid conversion of 4-NP to 4-aminophenol (4-AP). The raw PC was converted to magnetic PC (m-PC) particles, which made PC particles separate easily for cycling use. This discovery would also have applications in continuous flow-fluid catalysis.

Keywords Fe-Mn nodules · Fermi's function · Flow-through experiment · 4-nitrophenol · Pelagic clay

Associate Editor: Jana Madejová

Supplementary Information The online version contains supplementary material available at https://doi.org/10.1007/s42860-023-00266-0.

P. Zhang · T. Liu · X. Sun · W. Ning · S. Miao (✉)
Key Laboratory of Automobile Materials of Ministry of Education, Solid Waste Recycling Engineering Research Center of Jilin Province, School of Materials Science and Engineering, Jilin University, Changchun 130022, China
e-mail: miaosd@iccas.ac.cn

Q. Liang · W. Zhang
Jilin Provincial International Cooperation Key Laboratory of High-Efficiency Clean Energy Materials, and Electron Microscopy Center, Jilin University, Changchun 130012, China

W. Li
Key Laboratory of Mineral Resources Evaluation in Northeast Asia, Ministry of Natural Resources, Changchun 130061, China

X. Shi (✉)
Laboratory for Marine Geology, Pilot National Laboratory for Marine Science and Technology, Qingdao 266200, China
e-mail: xfshi@fio.org.cn

X. Shi
Key Laboratory of Marine Geology and Metallogeny (MNR), First Institute of Oceanography (MNR), Qingdao 266061, China

Introduction

Aromatic nitro compounds, which are very toxic, have been used widely in various fields, e.g. paper, pharmaceutical, and leather production (Ganguly et al., 2017). Humans suffer headaches and nausea after exposure to 4-nitrophenol (4-NP), and prolonged periods of exposure would damage the nervous system and even result in death (Reijnders, 2006). To address these issues, methods of chemical degradation, biological treatment and advanced oxidation have been developed by utilizing chemical reactions and photo-catalytic oxidation/reduction, e.g. using $NaBH_4$ as a reducing agent (Xiong et al., 2019). By transferring electrons to 4-NP molecules during the hydrolysis of $NaBH_4$, a less toxic product of 4-aminophenol (4-AP) would be obtained (Boran et al., 2013; Das & Das, 2022; Duong Dinh & Lin, 2018). Nevertheless, reactions always deteriorated by the slow kinetics due to mutually repulsive anions of 4-nitrophenolate and BH_4^- anions (Wu et al., 2017). The introduction of catalysts for efficient reduction of 4-NP is needed, therefore.

Transition metals in form of clusters that belong to the 'd_n' electron configurations have been used widely as catalysts for various reactions. The vacant d-orbital facilitates electron transfer from donor to acceptor molecules (Din et al., 2020; Zhao et al., 2015). The catalytic activity is revealed by the first-row transition metal oxides (Mandlimath & Gopal, 2011) and precious metals (Mejia & Reddy Bogireddy, 2022), e.g. catalysts of Au (Lin et al., 2013; Yan et al., 2020), Ag (Das et al., 2018a, 2018b, 2023), Pd (Suwannarat et al., 2018), Pt (Tuo et al., 2017), and Ru (Liu et al., 2018) have been found. Among these catalysts, iron oxides and their corresponding compounds, particularly the natural minerals/rocks containing Fe species, have been used widely as catalysts due to their vast abundance. The iron-bearing fly ashes have been demonstrated to catalyze the reduction of 4-NP, but the efficiency needs to be improved (Elfiad et al., 2018). Moreover, the performances of most solid wastes were unsatisfactory because of the tendency to deactivate in short periods of time (Xiong et al., 2019). Materials such as mesoporous silica (Das et al., 2018a, 2018b; Huang et al., 2020; Yan et al., 2014), fibers (including carbon and unwoven fibers) (Ullah et al., 2019; Yang et al., 2019), and minerals (Imangaliyeva et al., 2019; Jiang et al., 2020; Kim & Bae, 2018; Park & Bae, 2018) have been chosen for loading of catalytic species. Examples were found as Au-loaded clay minerals with incorporated Fe_3O_4 (Mu et al., 2014), iron oxides (Fe_xO_y) (Fu et al., 2021), Fe_xO_y-containing minerals (Park et al., 2020), and other Fe-based materials. Common features found in these materials were large surface areas, large capacity for physical adsorption, and surface activity. Fortunately, the natural clays have all of these features. Clays have excellent cation exchange capacity (CEC) because of electronegativity. The adsorption capacity of 4-NP was improved significantly due to the large CEC (Zermane et al., 2010). Clay catalysts supported with iron oxides (Zhang et al., 2010), iron clathrates (Ayodele & Hameed, 2013), and atomic-level iron (Gao et al., 2013) have great influence on the degradability of 4-NP. The performance originates from 'd_n' elements in these clay minerals. The activity of clay-based catalysts accelerated the adsorption of 4-NP as well as facilitating electron transfer. It was difficult to achieve Fe-doping at the atomic scale when Fe_xO_y nanoparticles were incorporated into clay minerals. In contrast, the Fe, Mn-rich pelagic clays are ideal for degradation of 4-NP because the raw Fe, Mn-rich pelagic clays (PC) were formed naturally, and have been verified (Zhang et al., 2022) to act as efficient Fenton catalysts due to their uniform distribution of Fe-Mn sites.

Metal-loaded clays have often been utilized for Fenton oxidation, but relatively few investigations have been conducted on Fenton-reduction catalysis. In this present study, pelagic clays were used directly as Fenton catalysts in the reduction of 4-NP with presence of $NaBH_4$. The S-shaped kinetics curve and possible mechanisms of catalytic reactions were proposed based on characterizations of Fourier-transform infrared spectroscopy (FTIR), X-ray photoelectron spectroscopy (XPS), and free Fe ions (Fe_{fr}) assay. The kinetics can be described as enzyme-like catalysis expressed by a Fermi's function. A fluid-flow experiment on a fixed-bed reactor was also carried out to test the feasibility of PC catalysts for practical applications; these can be envisaged as continuous catalysis applications for wastewater treatment.

Materials and Methods

Materials and chemicals

Five samples of pelagic clay collected from the Indian Ocean (labeled as #1, #2, #3, #4, and #5) were tested

https://doi.org/10.1007/s42860-023-00266-0 Published online by Cambridge University Press

in these experiments. Specimens PC #1–#4 were siliceous clays with large Fe and Mn contents (calculated as Fe_2O_3 and MnO, Table 1). The fifth specimen (PC #5) was a calcareous pelagic sediment containing less Fe and Mn (see Table 1). For comparison, another type of clay known as black cotton clay (BCS) a non-pelagic clay, which also has a large Fe content (collected from Kenya, details provided by Miao et al. (2018)), and two other commercially available clay minerals, illite (Ilt) and montmorillonite (Mnt), purchased from Aladdin Reagent Co. (Shanghai, China), were also tested for catalytic conversion of 4-NP with the assistance of incorporated Fe_3O_4 particles. The chemical compositions of the natural clays (PCs and BCS) are listed in Table 1. The clays above were air-dried in the laboratory at room temperature, and were ground by hand with an agate mortar and pestle into powders (100 mesh). Other reagents included commercial iron (Fe(0)) powders (99.9% metals basis, 300–500 nm), ferrous chloride tetrahydrate ($FeCl_2{\cdot}4H_2O$), ferric chloride hexahydrate ($FeCl_3{\cdot}6H_2O$), sodium hydroxide (NaOH), sodium carbonate (Na_2CO_3), sulfuric acid (H_2SO_4, 98%), 4-nitrophenol (4-NP), and sodium borohydride ($NaBH_4$) all of which were purchased from Beijing Chemical Works (Beijing, China). All reagents above including chemicals listed in the supporting information (SI) were of analytical grade and used without further purification.

Catalytic reduction of 4-NP and material characterizations

The typical experiment for catalytic reduction of 4-NP was performed by adding 18.9 mg of $NaBH_4$ (25.0 mM) to 20 mL of 4-NP (0.10 mM) in an aqueous solution. Subsequently, 4.0 mg of the air-dried PC (0.20 g/L) or other tested catalyst particles (Fe_3O_4/BCS, Ilt, and Mnt) were added to this solution to initiate the catalytic reactions. After arbitrary periods of time, a portion of the dispersion was removed and centrifuged (HC-3514 instrument, Ustc Zonkia Scientific Instruments, Hefei, Anhui, China; 21000 rpm, 27000 × g)) for analysis. The supernatant was measured by UV–Visible (UV–Vis) absorption on a spectrometer (Model T6, Beijing General Analytical Instrument, Beijing, China). The conversion efficiency of 4-NP was evaluated by recording absorbance at the typical wavelength of 400 nm.

Material characterizations included: X-ray diffraction (XRD, type DX-2700, Dandong Fangyuan Instrument Co., Dandong, Liaoning, China), Fourier-transform infrared spectroscopy (FTIR, Nicolet 380, Thermo Scientific, Madison, Wisconsin, USA), X-ray photoelectron spectroscopy (XPS, ESCALAB MK-II, VG industries co., New York, USA), scanning electron microscopy (SEM, JSM-6700F, JEOL, Akishima, Tokyo, Japan), transmission electron microscopy (TEM, JSM-2100F, JEOL, Akishima, Tokyo, Japan), stereo light microscopy (SLM, SMZ800N, Nikon, Tokyo, Japan), and UV–Vis absorption (Model T6, see above). The control experiment details (synthesis of Fe_3O_4 nanoparticles, determination of free Fe^{2+} in solution) and the standard curves for calculation are provided in the supporting information (SI, Fig. S1).

Results and Discussions

Catalytic performance of PC catalysts

The typical catalytic performance of pelagic sediments (PC#1), examined at the initial concentrations of 4-NP and $NaBH_4$, were 0.1 mM and 25.0 mM, respectively. The color change was observed from light yellow to

Table 1 Chemical compositions of the five samples of pelagic clays (PC #1–#5) and the black cotton clay (BCS) collected from Kenya

Oxide (wt.%)	SiO_2	Al_2O_3	Fe_2O_3	MnO	K_2O	Na_2O	CaO	MgO	Others
#1	24.20	7.80	25.95	7.05	2.68	10.35	9.65	1.71	10.61
#2	30.56	9.67	21.68	6.17	3.18	7.37	9.87	2.05	9.45
#3	39.35	12.17	18.74	4.95	3.02	7.92	2.38	3.07	8.40
#4	45.56	14.28	11.44	3.43	3.29	7.86	3.09	3.06	7.99
#5	10.24	1.42	2.10	0.81	0.37	2.56	79.54	0.74	2.22
BCS	50.34	16.98	9.40	0.06	1.00	0.79	1.60	1.11	18.70

https://doi.org/10.1007/s42860-023-00266-0 Published online by Cambridge University Press

bright yellow (Fig. S2), and the absorption peak was red-shifted from ~317 nm to ~400 nm after adding $NaBH_4$ (Fig. 1a). This was due to the fact that the solution pH increased from neutral to ~10.0, and the 4-NP molecules changed into 4-nitrophenolate ions with the addition of $NaBH_4$ (Jiang et al., 2020; Mohammadnezhad & Ariaeinezhad, 2021). The absorbance peak at ~400 nm remained constant, and solution color remained bright yellow in the absence of PC, proving that 4-nitrophenolate ions were not reduced if the PC particles were not added (as shown in Figs S2b, S5a). In contrast, the UV–Vis absorbance at $\lambda = 400$ nm decreased quickly (Fig. 1b), and the color of 4-NP changed to colorless when PC particles were added to the solution and used as catalysts. A video recording of the in situ change of the UV–Vis spectra (link at the end of this paper), demonstrates the outstanding performance of the PC within 720 s. Along with a reduction of the absorbance at 400 nm, a new peak appeared at 300 nm which represented the formation of 4-AP. The degradation of 4-NP was not prominent during the first 2.0 min (Fig. 1c), revealing that the catalytic reaction required a so-called induction time (λ, usually < 2.0 min). After this induction period, the reaction was accelerated and the intensity of the peak at 400 nm declined rapidly, suggesting the degradation was rapid after the induction period. Almost all of the 4-NP was converted to 4-AP within ~480 s, which were confirmed by the color change from bright yellow to colorless (Fig. S2). This result suggested that PC was very efficient at the catalytic reduction of 4-NP.

As the catalytic reaction progressed, the brown-colored PC particles turned black which indicated that magnetic clay (m-PC) particles were produced (Fig. S2e,f). The SLM images also illustrated an increase in the number of magnetic black particles (Fig. S3). The black m-PC particles, however, were unstable and easily transformed back into brown-colored when the m-PC was treated by washing/drying procedures, especially when particles were exposed to air. The conversion percentage reached 100% within 780 s when samples PC #1–#4 were

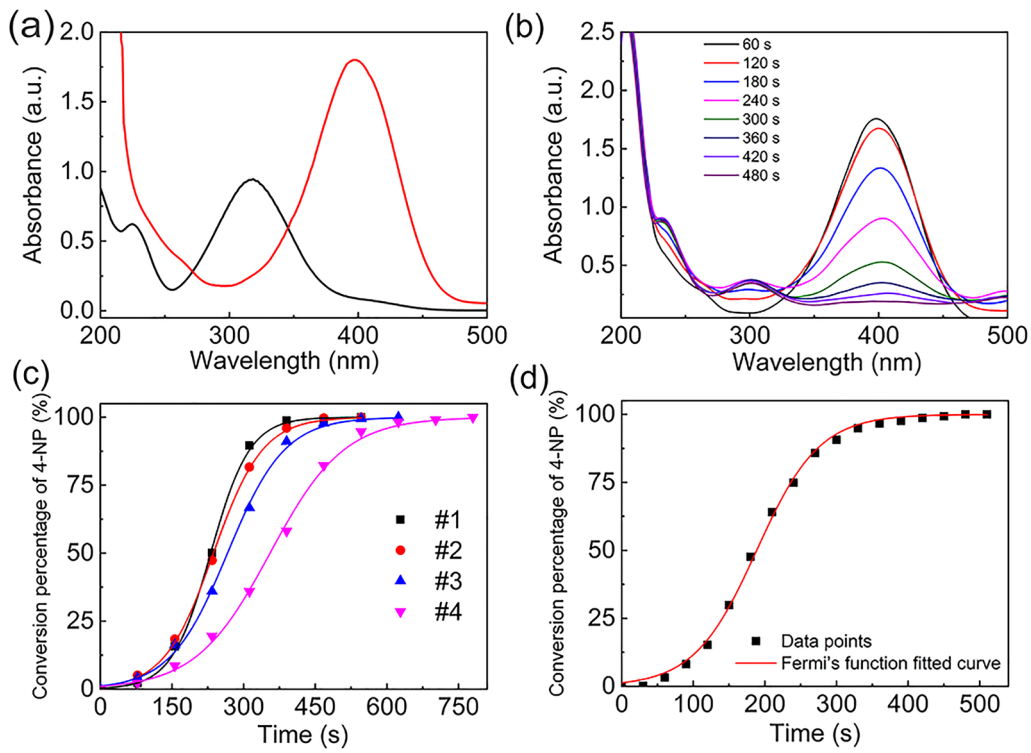

Fig. 1 **a** UV–Vis spectra of 4-NP solution before and after addition of $NaBH_4$; **b** UV–Vis spectra showing reduction of 4-NP with time after addition of PC; **c** plots showing the conversion efficiency of 4-NP to 4-NP with added PC (#1–#4); and with **d** Fermi's function fitted to the plot of conversion of 4-NP vs. time which was catalyzed by pelagic clays (PC #1). Dosages for the catalysis reaction were 0.10 mM 4-NP, 25.0 mM $NaBH_4$, and 0.20 g/L PC

https://doi.org/10.1007/s42860-023-00266-0 Published online by Cambridge University Press

used as fresh catalysts (Fig. 1c). In case of PC#5, only 10.0% conversion of 4-NP was achieved within 20.0 min (Fig. S4). The catalytic efficiency of the five samples followed the order #1 > #2 > #3 > #4 > #5, suggesting that the pelagic clays with larger larger Fe- and Mn contents showed better catalytic performance.

Traditionally, the conversion percentages (η) of 4-NP by $NaBH_4$ is as described in Eq. 1. The pseudo-first order kinetics expressed as Eq. 2 described the reaction for metal catalysis, which was of zero-order by considering the concentration of 4-NP with respect to an excess amount of $NaBH_4$ (Chen et al., 2020; Jiang et al., 2020).

$$\eta\ (\%) = 100(C_0 - C_t)/C_0 \tag{1}$$

$$\ln\left(\frac{C_t}{C_0}\right) = -kt \tag{2}$$

In Eqs. 1 and 2, C_0 and C_t are the initial and instant concentrations of 4-NP at time t, and k is the apparent rate constant. This indicates that the 4-NP consumed in the form of C_t/C_0 varied with time (t) exponentially. For most metal catalysts, the two-step pseudo-first order model was always used to determine rate constant k (Wunder et al., 2010). However, the kinetics curve of 4-NP degradation catalyzed by the PC in the present system was S-shaped, which varies slightly from that of metal catalysts (Wunder et al., 2010). The reason may be the simultaneous occurrence of 4-NP degradation that followed the 'induction period' during catalysis. Therefore, an alternative model, the Fermi function (Eq. 3), was proposed to fit the kinetics of degradation catalyzed by PC (Minz et al., 2018):

$$\eta(\%) = 100/(1 + \exp(-k(t - t*))) \tag{3}$$

where η is the conversion percentage of 4-NP, k is the apparent rate constant, and t* is the transition time. The conversion curves were generally fitted in a symmetrical style, and the position of t* determines the period of inflection point in the S-shaped curve, which corresponded to the maximum rate (μ_m). Therefore, the period of t* is called the lag phase and was appointed as an exponential parameter. According to Ware and Power (2017), the S-shaped kinetics was always modulated as bacterial growth to describe superior kinetics catalyzed by enzyme-processes. Thus, the PC catalysis in the present system was assumed to be an enzyme-like process with great efficiency. The degradation curve is further characterized by introducing the parameter λ as the induction time, which is the intersection of curve slope with the X-axis (Zwietering et al., 1990). The equations (Eqs. 4&5) were listed as follows:

$$\mu_m = k/4 \tag{4}$$

$$\lambda = t^* - 2/k \tag{5}$$

where λ is given by the intercept of the curve with the X-axis.

The equations above were used to fit the degradation of 4-NP for reaction conditions of 0.1 mM 4-NP, 25.0 mM $NaBH_4$, and 0.2 g/L PC#1. Parameters derived from the typical fitted curve (Fig. 1d) were $k = 27.53 \times 10^{-3}\ s^{-1}$, $t* = 188.43$ s, $\mu_m = 6.11 \times 10^{-3}\ s^{-1}$, $\lambda = 101.2$ s, and $R^2 = 0.9991$. The model provided accurate quantification on both induction time (λ) and the maximum degradation rate (μ_m). The coefficient of determination (R^2) of catalysis using PC #1–#4 was in the range 0.9983–0.9991 (Fig. 1c, Table 2), suggesting a good match of Fermi's function. As can be seen, the values for k and μ_m increased and λ decreased with increasing Fe and Mn contents.

The PC dosage, pH, and initial concentrations of 4-NP and $NaBH_4$ in the reaction solutions affect 4-NP degradation performance (Table 3). The k values increased from $24.43 \times 10^{-3}\ s^{-1}$ to $31.87 \times 10^{-3}\ s^{-1}$ (Fig. 2a) with incremental dosages of PC particles from 0.1 to 0.3 g/L. The pH values ranging from 4.0 to 8.0 were examined to study the influence of pH on the reaction kinetics. The k value was $78.99 \times 10^{-3}\ s^{-1}$ at a pH of 4.0, which was much greater than that of pH 7.0 (Figs 2b, S5c). With increasing concentration of 4-NP from 0.05 to 0.2 mM, the kinetic constants (k) decreased from $43.34 \times 10^{-3}\ s^{-1}$ to $9.31 \times 10^{-3}\ s^{-1}$ (Fig. 2c), indicating that the reaction rates were very influenced by the initial concentration of 4-NP. When the initial concentrations of $NaBH_4$ increased from 10.0 to 75.0 mM, k values increased from $3.58 \times 10^{-3}\ s^{-1}$ to $44.47 \times 10^{-3}\ s^{-1}$ (Figs 2d, S5b)). The value of k increased, μ_m increased, and the induction time λ decreased, which is consistent with the accelerated kinetics. The range of R^2 was always found to be between 0.9985 and 0.9995, illustrating the accuracy of using Fermi's equation in describing all reactions in the catalytic conversion of 4-NP when the PC

https://doi.org/10.1007/s42860-023-00266-0 Published online by Cambridge University Press

Table 2 Parameters derived from Fermi's function by using pelagic clays (PC #1–#4) as catalysts in the conversion of 4-NP

Sample No	4-NP (mM)	$NaBH_4$ (mM)	PC (g L^{-1})	k ($\times 10^{-3}$ s^{-1})	t^* (s)	μ_m ($\times 10^{-3}$ s^{-1})	λ (s)	R^2
#1	0.1	25.0	0.2	24.43	188.43	6.11	101.21	0.9991
#2	0.1	25.0	0.2	22.93	231.00	5.73	149.13	0.9985
#3	0.1	25.0	0.2	16.65	266.14	4.16	146.02	0.9986
#4	0.1	25.0	0.2	12.83	355.18	3.21	199.29	0.9983

Table 3 Factors affecting degradation of 4-NP and derived parameters from Fermi's function

PC (g L^{-1})	pH	4-NP (mM)	$NaBH_4$ (mM)	k (10^{-3} s^{-1})	t^* (s)	μ_m (10^{-3} s^{-1})	λ (s)	R^2
0.1	7.0	0.1	25.0	27.53	250.01	6.88	177.36	0.9993
0.2	7.0	0.1	25.0	24.43	188.43	6.11	101.21	0.9991
0.3	7.0	0.1	25.0	31.87	159.00	7.97	96.25	0.9998
0.2	4.0	0.1	25.0	78.99	47.91	19.75	22.59	0.9992
0.2	7.0	0.1	25.0	24.43	188.43	6.11	101.21	0.9991
0.2	10.0	0.1	25.0	2.73	1915.20	0.68	1182.60	0.9985
0.2	7.0	0.05	25.0	43.34	139.82	10.80	93.68	0.9995
0.2	7.0	0.1	25.0	24.43	188.43	6.11	101.21	0.9991
0.2	7.0	0.2	25.0	9.31	355.53	2.33	140.70	0.9987
0.2	7.0	0.1	10.0	3.58	860.06	0.90	301.15	0.9921
0.2	7.0	0.1	25.0	24.43	188.43	6.11	101.21	0.9991
0.2	7.0	0.1	50.0	27.44	181.99	6.86	109.11	0.9966
0.2	7.0	0.1	70.0	44.47	113.03	11.12	68.06	0.9991

particles were used as catalysts. These results also indicated that the initial concentration of $NaBH_4$ was excessive compared with 4-NP; the small variation in $NaBH_4$ concentration thus had less impact on the 4-NP conversion. The color of 4-NP solution always changed from light yellow to colorless (Fig. S2d) when the initial solution of 4-NP was acidic (pH 4.0). The leaching of metal ions in PC and hydrolysis of $NaBH_4$ were more susceptible in an acidic environment, which accelerated the enzyme-like catalysis by PC. The induction time decreased significantly (Fig. S5d). Considering the influence of factors above, a better dosage of PC#1 for conducting the catalytic reduction of 4-NP (0.1 mM 4-NP, 25.0 mM $NaBH_4$) should be 0.2 g/L, and the pH value of the reaction solution was 7.0. To illustrate the superiority of PC, a survey of literature for various catalysts used to catalyze 4-NP reduction by $NaBH_4$ was done. The catalytic ability of PC was superior to most of the reported catalysts (Table S1).

To study the recyclability of the PC catalyst, the m-PC was retrieved by washing, then drying either with or without exposure to air. The PC particles were separated from the solution with a magnet and reused for the next run of catalysis. When samples were washed and dried in air, an increase in reaction time in the next run of catalysis was observed, i.e. the activity was inferior to the fresh sample (Table S2). For example, the conversion percentage of 4-NP during the 3rd-catalytic reaction cycle was 83.38% with 60 min of reaction time (Fig. 3a). The magnetic particles (m-PC) transformed back to non-magnetic particles if the sample was air dried, but the kinetics curve of 4-NP during the cycling catalysis still remained S-shaped. If the sample was used without exposure to air, the degradation time of 4-NP increased gradually from 8.0 to 45.5 min after five consecutives reuses (Fig. 3b). Although the PC catalysts were deactivated during reuse, they could be reactivated by prolonged time in the mother solution of 4-AP + $NaBH_4$. The

https://doi.org/10.1007/s42860-023-00266-0 Published online by Cambridge University Press

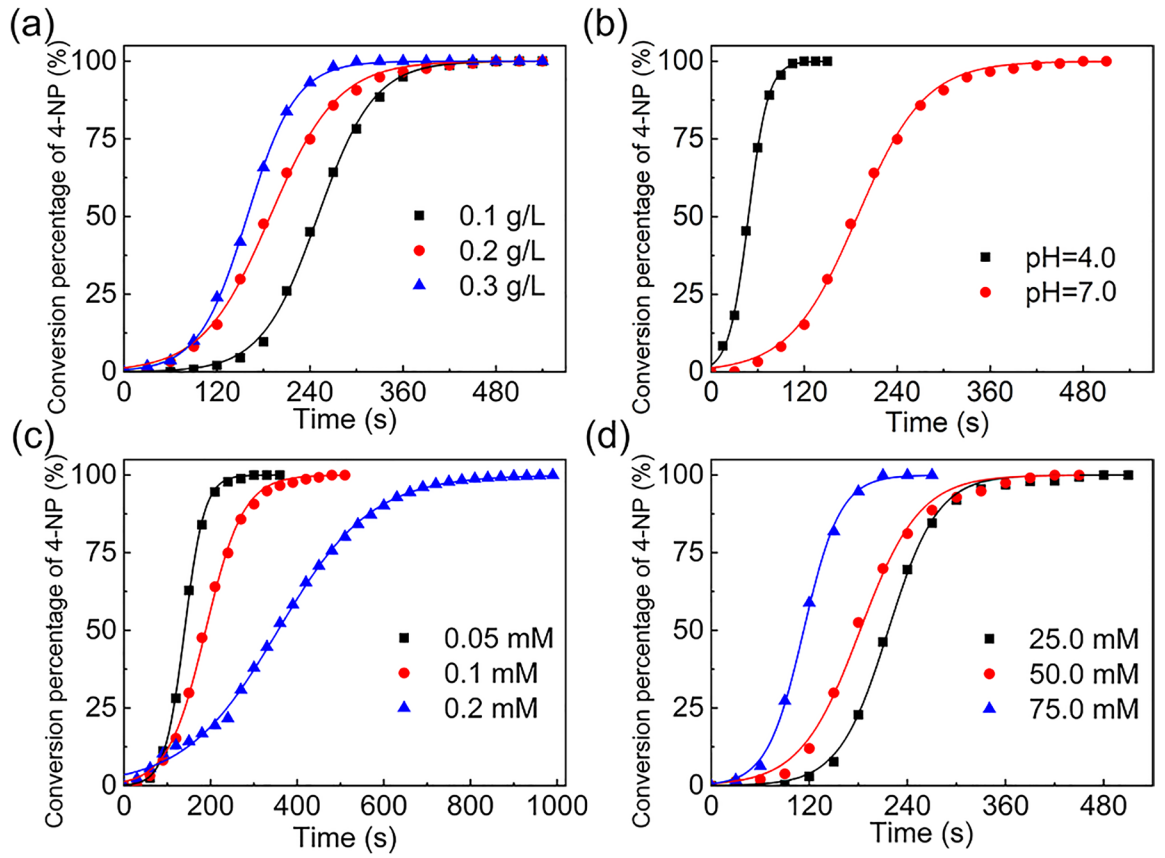

Fig. 2 Plots of the conversion percentage of 4-NP versus time, illustrating various factors that affect the reaction kinetics, including **a** dosages of PC, **b** initial pH (4.0 or 7.0) of the aqueous solution of 4-NP + $NaBH_4$, **c**, **d** initial concentrations of 4-NP **c** and $NaBH_4$ **d**

m-PC particles were kept in the mother solution for 5.0 h before reclaiming the PC, then removed with precautions to avoid oxidation to be reused in subsequent catalysis runs. The degradation time for complete conversion of 4-NP was 8.0 min, 6.5 min, 6.5 min, 7.8 min, and 11.7 min for the 1^{st}- to 5^{th}-cycles of PC catalysis (Fig. 3c, d). Certainly, the catalytic activity of the fresh sample remained relatively good (Fig. S6), indicating that the prolonged time for preserving PC stabilizes active sites in the reducing environment of the mother solution.

To perform the fixed-bed catalysis, a length (20.0 mm) of skim cotton and 2.0 mm thick PC were loaded in a glass tube (L = 20.0 mm, ϕ = 6.0 mm), and the catalysis was carried out by flowing a mixed solution of 4-NP and $NaBH_4$ (Fig. S7). The variation of UV–Vis absorption spectra and conversion percentages of 4-NP collected at different flow rates (Fig. 4) revealed that, with an increase in flow rate from 2.11 to 3.30 mL/min, the conversion efficiency of 4-NP declined from 100% to 99.0%, which meant a complete conversion of 4-NP through this fixed bed. The result indicated that the PC catalyst had the ability to catalyze the conversion of the 4-NP in a continuous flow process. When the flow rate was accelerated, the contact time between 4-NP molecules and PC particles decreased, resulting in incomplete conversion of 4-NP. Based on the experiment, the optimum flow rate for the fixed bed of 4-NP should be ≤2.50 mL/min in the fixed bed of the column.

Material characterization

XRD patterns of the five raw pelagic clays illustrated that all samples were almost identical except for the relative intensity of diffraction peaks indexed

https://doi.org/10.1007/s42860-023-00266-0 Published online by Cambridge University Press

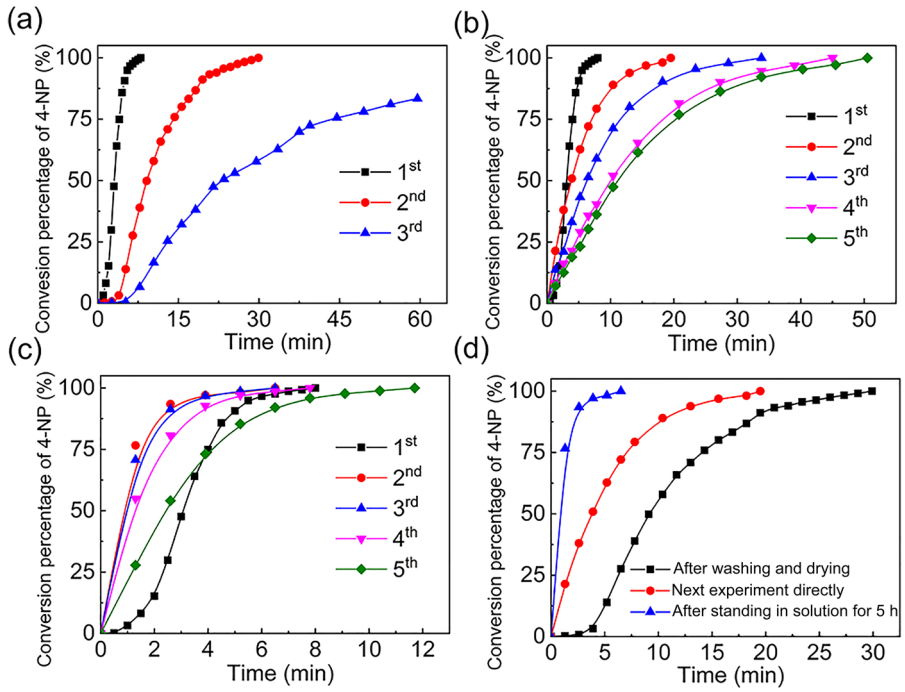

Fig. 3 Plots of the conversion percentage of 4-NP versus time during the reuse of PC particles as catalysts that were reclaimed via various methods: **a** the PC sample reclaimed after water-washing and air-drying; **b** PC was reused immediately after the previous run of catalysis without exposure to air; **c** PC was preserved in the 4-NP solution for ~5.0 h before the next run of catalysis; and **d** plots showing performance by comparison of the 2nd catalysis using PC reclaimed by the three means above

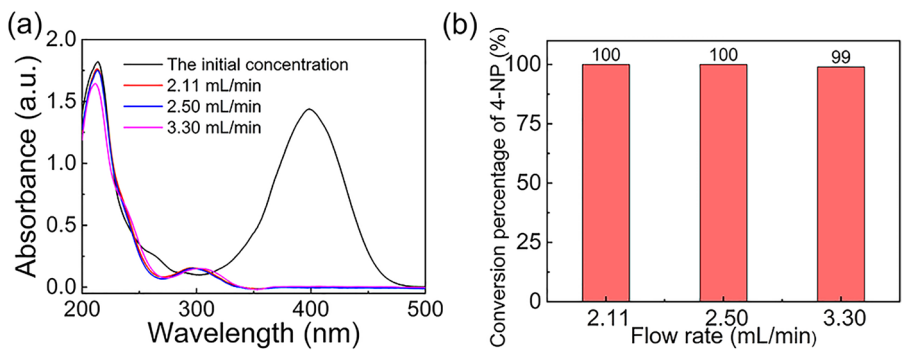

Fig. 4 **a** UV–Vis spectra of solution of 4-NP and $NaBH_4$ collected from the fixed bed after catalyzing at various flow rates (2.11, 2.50, and 3.30 mL/min), and **b** conversion percentage of 4-NP solution tested at various flow rates

to rock-forming minerals, e.g. quartz, feldspar, etc. (see Fig. S8). For PC#1 to #4, the main reflections appeared at 12.4º2θ (d_{001} = 7.13 Å) and 25.0º2θ (d_{002} = 3.56 Å), indicating the low crystallinity of kaolinite present in the PC. According to the XRD analysis (Fig. S8) and chemical compositions (Table 1), Fe and Mn are probably present primarily as amorphous phases which may be hydroxide phases or the so-called Fe-Mn nodules (Banerjee et al., 1999; Sensarma et al., 2016). Well crystallized calcite was observed as in the main mineral in sample PC#5, which indicated that the geological environment of PC#5 was different from samples PC#1–PC#4.

https://doi.org/10.1007/s42860-023-00266-0 Published online by Cambridge University Press

The ex-situ variation of PC structures during catalysis was studied by using XRD. The diffraction peaks at ~25.0º2θ were broader (Fig. 5a), suggesting structural transformation from the poorly crystalline kaolinite to more amorphous features. The structural transformation seemed to be reversible when the sample was collected from the reaction solution and exposed to air. This could be explained by the fact that PC was reduced by $NaBH_4$, and the clay structure was slightly collapsed. When the PC was re-oxidized, the structure of PC was reconstructed after exposure to air. The FTIR spectrum of the PC sample after the catalytic reaction gained a new absorption peak at 1500 cm^{-1}, which was the amino vibration of 4-AP (Fig. 5b), indicating that the degradation of 4-NP occurred on the surface of PC, and the 4-AP products were partially adsorbed and blocked the active sites of PC particles.

SEM and TEM were used to characterize the morphology of the PC and the m-PC (Figs. 6, 7). As can be seen, mixed-layer illite-montmorillonite, feldspar, spherical Fe-Mn nodules, and clay layers were all observed (Fig. S9). In accordance with the XRD characterization, the mixed-layer illite-montmorillonite layer in PC was in the range 2.0–3.0 μm with rough surfaces, exhibiting broken and curled edges (Fig. 6). This morphological feature would expand the specific surface area, and would promote more active sites for degradation of 4-NP. The TEM images (Fig. 7a-7c) indicated the complicated composition/mineralogy of the PC. Although the surface curls and clusters of the PC were shape-altered as the cyclic reaction proceeded, most of the layered structures of the pelagic clays were preserved after the reaction (Fig. 7d–f), suggesting that the stability of clay minerals was significant during the catalysis.

The surface chemistry of PC before and after the reaction was investigated by XPS. The Fe 2p band (Fig. 8a) implied that species of Fe were present both as Fe(III) and Fe(II). The XPS bands at 709.9 and 723.4 eV, and satellite peaks at 715.5 and 728.1 eV, were attributed to the Fe(II). Bands at 711.2 and 725.0 eV and the satellite peaks at 719.0 and 733.0 eV were attributed to Fe(III) (Wan et al., 2015; Wang et al., 2021). The amount of Fe(II) increased with progress in the catalysis. Based on the integrated area of deconvoluted bands, ratios of the two oxidation states Fe(II):Fe(III) were evaluated to be 0.37:1, 0.52:1, and 0.80:1 from the beginning to end of the reaction. Both oxidation states of Mn(III) (642.3 eV) and Mn(IV) (641.3 eV) were also detected in raw PC (Díaz-Arriaga et al., 2020; Wang et al., 2021). A new characteristic band was observed at 640.4 eV, however (Fig. 8b), which can be assigned to the Mn(II) state, and the amount of this type of manganese increased progressively with reduction of 4-NP (Grissa et al., 2017). When the reaction was completed, the ratio of Mn(II), Mn(III), and Mn(IV) was determined to be 1.03:0.89:1. This might be due to the much lower valence states (Fe(II) and Mn(II)) produced in the PC with the presence of $NaBH_4$. This can also be used to explain the magnetic variation between PC and m-PC, and the appearance of the lag phase and S-shaped curve of the 4-NP conversion was found in the case of m-PC. No variations in the XPS bands from Si 2p and Al 2p were observed before or after the reaction (Fig. S10). This indicated that the Fe and Mn species played roles in the 4-NP reduction. Unfortunately,

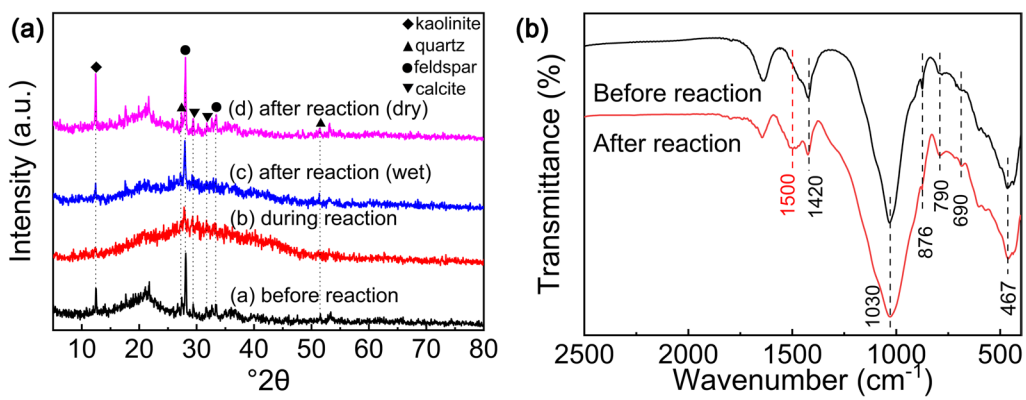

Fig. 5 **a** The XRD patterns of the PC samples collected before (raw clay), during, and after the catalytic reduction of 4-NP; and **b** FTIR spectra of PC before and after catalytic reaction

https://doi.org/10.1007/s42860-023-00266-0 Published online by Cambridge University Press

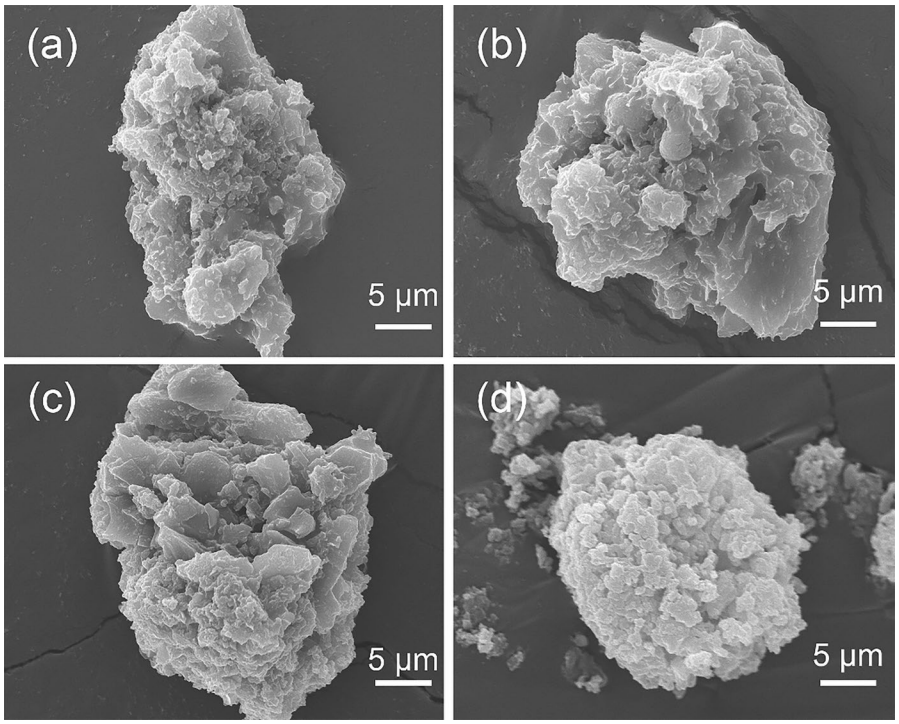

Fig. 6 SEM images of **a** the raw pelagic clays, and **b–d** the reused pelagic clays after various numbers of cycles of use: **b** the 1st, **c** 2nd, and **d** 5th run of catalysis

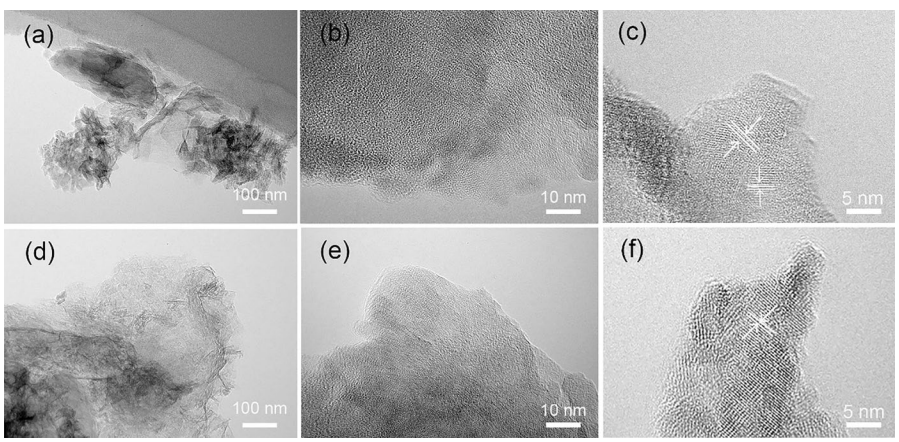

Fig. 7 TEM images of the pelagic clay samples used before **a–c** and after **d–f** the catalytic reduction of 4-NP

due to the poor crystallinity of Fe- and Mn-nodules, the XRD spectra could not give better evidence.

The assay of free Fe^{2+} ions (Fe_{fr}) that might be dissolved from PC was tested using 1,10-phenanthroline as the indicator. Four types of mother solutions 'PC + $NaBH_4$ + 4-NP', 'PC + $NaBH_4$', '$NaBH_4$ + 4-NP', and 'PC + 4-NP' were tested for time-released Fe^{x+} ions (tested as Fe^{2+}, see SI). Only systems of 'PC + $NaBH_4$ + PC' and 'PC + $NaBH_4$' were found to contain Fe_{fr} (Fig. S11). This indicated that part of the Fe-species was released into solution with the presence of $NaBH_4$. The curve of the Fe^{2+} concentration

https://doi.org/10.1007/s42860-023-00266-0 Published online by Cambridge University Press

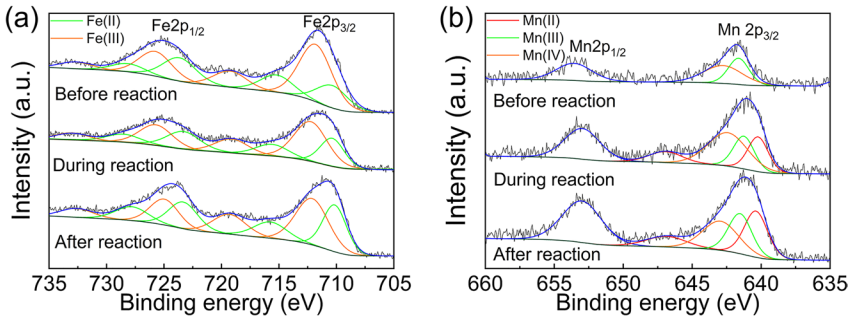

Fig. 8 **a** The high-resolution XPS spectrum and deconvoluted curves of Fe 2p, and **b** Mn 2p of pelagic clay before, during, and after the catalytic reduction of 4-NP using $NaBH_4$

of the whole reaction (Fig. 9) revealed that the change of Fe_{fr} concentration in solution was roughly S-shaped, which was similar to the 4-NP conversion curve. The Fe_{fr} concentration decreased gradually after the reaction, presumably due to the Fe_{fr} being fixed back into the clay particles, which could also be illustrated by the Fe_{fr} concentration at different time in different systems (Fig. S12). The raw PC was a superior enzyme-like catalyst in the conversion of 4-NP to 4-AP with the presence of $NaBH_4$.

Proposed reaction mechanisms

The catalytic efficiency depends on both the activated species and surface adsorption of the substrate molecules/ions according to the Langmuir–Hinshelwood pathway (Wunder et al., 2010). In the catalytic reaction, the surface activation during the induction period was assumed to be

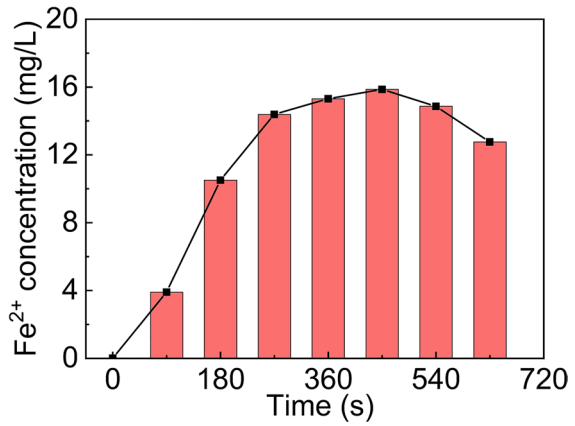

Fig. 9 The Fe^{2+} concentration in the solution (PC + $NaBH_4$ + 4-NP) during degradation

the initial step, i.e. a reduction of the Fe-Mn amorphous nodules with assistance of $NaBH_4$. Some low-valence ions in the catalyst would be transferred to active sites at the surface, and ~2.75% of the Fe-species was released into the solution/dispersion. The layered structure of clay minerals provided an ideal support for activation of the clay surface and adsorption of 4-nitrophenol and borohydrides. This type of structure would facilitate electron transfer as well as enhance the catalytic performance (Menumerov et al., 2016). Based on the characterization of PC samples, the present authors concluded that the induction time was related to dynamic surface activation. This activation of Fe-Mn active sites and adsorption of borohydride and 4-nitrophenol ions were indicated to take place on the PC surface (Minz et al., 2018; Wunder et al., 2010). Based on the characterizations above, a proposed reaction mechanism could be postulated (Fig. 10). With addition of $NaBH_4$, the 4-NP molecules were converted rapidly to 4-nitrophenol ions; meanwhile the clay minerals were converted to black magnetic m-PC (Fe(0)) by $NaBH_4$. At the same time, ions of BH_4^- lost electrons and converted to HBO_3^- which can be described as Eqs. 6–9. The Fe(0) and Mn(II) obtained from the PC during the reduction would participate in the degradation process (4-NP→4-AP), but these low-valence Fe- or Mn-species would be re-oxidized to Fe(II) and Mn(III) (Fig. 10a) again when the suspension was exposed to air. For the subsequent cycles of reusing PC, the activated PC particles were able to catalyze the reaction directly under condition that the reclaimed m-PC was not oxidized (Fig. 10b). Otherwise, the re-oxidized PC particles have to be activated again in the reductive environment. With assistance of the activated m-PC, the 4-nitrophenol ions and BH_4^- ions were adsorbed on the Fe-Mn sites, and the electronic transfer would take place. Following the Langmuir–Hinshelwood pathway,

https://doi.org/10.1007/s42860-023-00266-0 Published online by Cambridge University Press

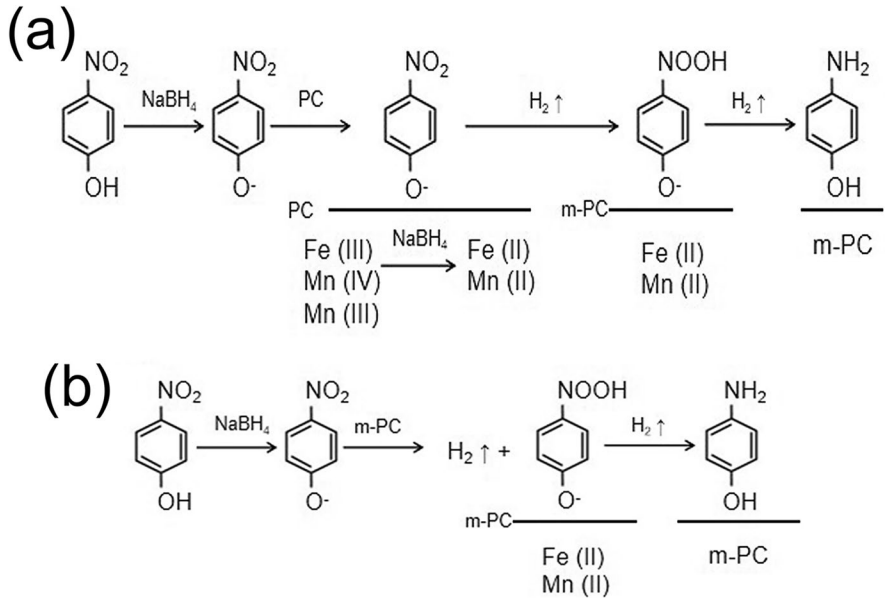

Fig. 10 The proposed reaction pathway catalyzed by **a** raw PC, and **b** m-PC for conversion from 4-NP to 4-AP

the reduction of 4-NP was indicated to involve collection and transport of electrons, and the continual reduction and immobilization of Fe and Mn species were of great importance. The PC with greater Fe and Mn contents exhibited greater catalytic activity. Therefore, our PC behaved as an efficient enzyme-like catalyst. The activation of PC and its simultaneous catalysis were ascribed to the efficiency that was described by an S-shaped kinetics plot.

$$BH_4^- + 3\,H_2O + 2\,Fe(III) \rightarrow 2Fe(0) + 6H^+ + H_2BO_3^- + H_2 \quad (6)$$

$$BH_4^- + 3H_2O + Mn(IV) + 2\,Mn(III) \rightarrow 3\,Mn(II) + 4H^+ + H_2BO_3^- + 2H_2 \quad (7)$$

$$4-NP + 3\,Fe(0) + 6H^+ \rightarrow 3\,Fe(II) + 2H_2O + 4-AP \quad (8)$$

$$4-NP + 4\,Mn(II) + 6H^+ \rightarrow 2\,Mn(III) + 2\,Mn(IV) + 2H_2O + 4AP \quad (9)$$

Comparison sample study

More crystalline BCS clays, as described in the Materials and Methods section, were also tested for their catalytic activity for a comparison purposes. The BCS contains a certain amount of Fe (Fe_2O_3, 9.40%). Two other types of clay minerals (Ilt and Mnt) with smaller Fe and Mn species contents were also used for comparison. The Fe and Mn contents in these clay minerals was less than those in PC. To increase the Fe content, commercial metallic iron powders (Fe(0)) and synthesized iron oxide (Fe_3O_4) nanoparticles were incorporated into BCS or other minerals to prepare composites, e.g. Fe(0)/BCS. The synthesis method for Fe_3O_4 is described in the SI. Only the composite of Fe(0)/BCS had certain catalytic performance, with a conversion efficiency of 89.97% after 360 min (Figs 11, S13). This result suggests that Fe(0) was the catalytic species. The curve could be fitted by first-order kinetics with $k = 0.11 \times 10^{-3}\ s^{-1}$, which was smaller than the PC. The results above confirmed the high catalytic ability of PC, which originates mainly from the amorphous Fe and Mn species in the pelagic clays.

Conclusions

In conclusion, the (Fe, Mn)-rich pelagic clay collected from the Indian Ocean was discovered to work as a high-activity, recyclable enzyme-like catalyst. The PC catalyzed the rapid conversion of 4-NP to 4-AP while PC was also transformed into

https://doi.org/10.1007/s42860-023-00266-0 Published online by Cambridge University Press

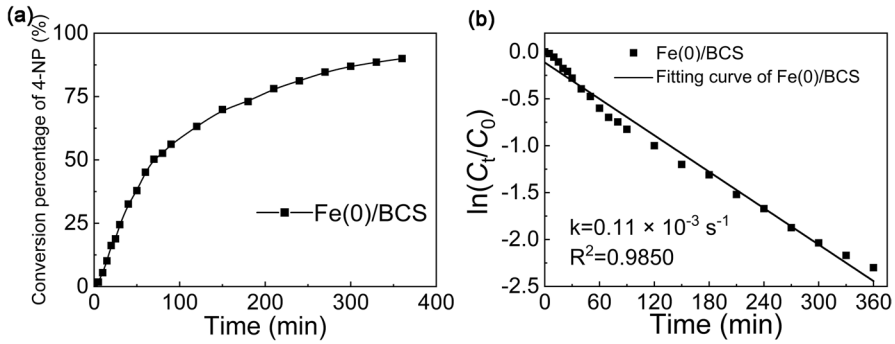

Fig. 11 **a** Plot of the degradation of 4-NP using Fe(0)/BCS as the catalyst, and **b** plot of $\ln(C_t/C_0)$ versus time, for the reduction of 4-NP using $NaBH_4$ as the reducing agent and Fe(0)/BCS as the catalyst

black magnetic particles in the $NaBH_4$ aqueous solution, which could be separated easily from the solution by magnetic separation. The structure and morphology of PC particles before, during, and after catalysis were characterized by XRD, FTIR, XPS, SEM, and TEM, which showed that only the valence state of Fe and Mn elements changed significantly. These results indicated that the Fe(III), Mn(IV), and Mn(III) in the PC were first reduced to the lower valence Fe(0) and Mn(II) by $NaBH_4$, which participated in the subsequent degradation of 4-NP in the catalytic process. This process was known as the induction time and simultaneous activation of the surface. Due to the induction time, the degradation of 4-NP yielded an S-shaped kinetics curve, and Fermi's equation model was employed to describe the catalysis. This model overcame the inaccuracy of the previous pseudo-first order kinetics descriptions. The apparent rate constant of PC ($k = 27.53 \times 10^{-3}$ s^{-1}) was much greater than those of other reported clay-based metal catalysts. The advantages of PC, such as being environmentally benign, highly efficient, and with no need for secondary treatment, make it an ideal candidate for various applications in water purification.

Acknowledgements The authors acknowledge financial support from the National Key Research and Development Program of China (2023YFC2811200), Marine S&T Fund of Shandong Province for Pilot National Laboratory for Marine Science and Technology (Qingdao) (2021QNLM020003-1), project of National Natural Science Foundation of China (52374266, 91858209), 'Mineralogical mechanism of SiO_2-rich kaolinite and development of new material technology (3R1210735415)', and 'Scientific and Technological Developing Scheme of Jilin Province (20200401028GX)'.

Data availability All the data and materials for this study are available herein.

Declarations

Conflict of Interest On behalf of all authors, the corresponding author states that there is no conflict of interest.

References

Ayodele, O. B., & Hameed, B. H. (2013). Development of kaolinite supported ferric oxalate heterogeneous catalyst for degradation of 4-nitrophenol in photo-Fenton process. *Applied Clay Science, 83*, 171–181. https://doi.org/10.1016/j.clay.2013.08.019

Banerjee, R., Roy, S., Dasgupta, S., Mukhopadhyay, S., & Miura, H. (1999). Petrogenesis of ferromanganese nodules from east of the Chagos Archipelago, Central Indian Basin, Indian Ocean. *Marine Geology, 157*(3–4), 145–158. https://doi.org/10.1016/S0025-3227(98)00156-X

Boran, A., Erkan, S., Ozkar, S., & Eroglu, I. (2013). Kinetics of hydrogen generation from hydrolysis of sodium borohydride on Pt/C catalyst in a flow reactor. *International Journal of Energy Research, 37*(5), 443–448. https://doi.org/10.1002/er.3007

Chen, M., Gao, Y., Fu, B., & Yang, F. (2020). A Tandem Adsorption-Catalysis Strategy for the Removal of Copper Ions and Catalytic Reduction of 4-Nitrophenol. *ACS Omega, 5*(36), 23372–23377. https://doi.org/10.1021/acsomega.0c03329

Das, T. K., & Das, N. C. (2022). Advances on catalytic reduction of 4-nitrophenol by nanostructured materials as benchmark reaction. *International Nano Letters, 12*(3), 223–242. https://doi.org/10.1007/s40089-021-00362-w

Das, T. K., Ganguly, S., Bhawal, P., Mondal, S., & Das, N. C. (2018a). A facile green synthesis of silver nanoparticle-decorated hydroxyapatite for efficient catalytic activity towards 4-nitrophenol reduction. *Research on Chemical Intermediates, 44*(2), 1189–1208. https://doi.org/10.1007/s11164-017-3161-7

Das, T. K., Ganguly, S., Bhawal, P., Remanan, S., Ghosh, S., & Das, N. C. (2018b). A facile green synthesis of silver nanoparticles decorated silica nanocomposites using mussel inspired polydopamine chemistry and assessment its catalytic activity. *Journal of Environmental Chemical Engineering, 6*, 6989–7001. https://doi.org/10.1016/j.jece.2018.10.067

Das, T.K., Ghosh, S.K., & Das, N.C. (2023). Green synthesis of a reduced graphene oxide/silver nanoparticles-based catalyst for degradation of a wide range of organic pollutants. *Nano-Structures & Nano-Objects,* 100960. https://doi.org/10.1016/j.nanoso.2023.100960

Díaz-Arriaga, C. B., Baas-López, J. M., Pacheco-Catalán, D. E., & Uribe-Calderon, J. (2020). Symmetric electrochemical capacitor based on PPy obtained via MnO_2 reactive template synthesis. *Synthetic Metals, 269*, 116541. https://doi.org/10.1016/j.synthmet.2020.116541

Din, M. I., Khalid, R., Hussain, Z., Hussain, T., Mujahid, A., Najeeb, J., & Izhar, F. (2020). Nanocatalytic Assemblies for Catalytic Reduction of Nitrophenols: A Critical Review. *Critical Reviews in Analytical Chemistry, 50*(4), 322–338. https://doi.org/10.1080/10408347.2019.1637241

Duong Dinh, T., & Lin, K.-Y.A. (2018). Ruthenium supported on ZIF-67 as an enhanced catalyst for hydrogen generation from hydrolysis of sodium borohydride. *Chemical Engineering Journal, 351*, 48–55. https://doi.org/10.1016/j.cej.2018.06.082

Elfiad, A., Galli, F., Djadoun, A., Sennour, M., Chegrouche, S., Meddour-Boukhobza, L., & Boffito, D. C. (2018). Natural alpha-Fe_2O_3 as an efficient catalyst for the p-nitrophenol reduction. *Materials Science and Engineering: B, 229*, 126–134. https://doi.org/10.1016/j.mseb.2017.12.009

Fu, M., Li, M., Zhao, Y., Bai, Y., Fang, X., Kang, X., Yang, M., Wei, Y., & Xu, X. (2021). A study on the high efficiency reduction of p-nitrophenol (4-NP) by a $Fe(OH)_3/Fe_2O_3$@Au composite catalyst. *RSC Advances, 11*(43), 26502–26508. https://doi.org/10.1039/D1RA04073A

Ganguly, S., Das, P., Bose, M., Das, T. K., Mondal, S., Das, A. K., & Das, N. C. (2017). Sonochemical green reduction to prepare Ag nanoparticles decorated graphene sheets for catalytic performance and antibacterial application. *Ultrasonics Sonochemistry, 39*, 577–588. https://doi.org/10.1016/j.ultsonch.2017.05.005

Gao, Y., Gan, H., Zhang, G., & Guo, Y. (2013). Visible light assisted Fenton-like degradation of rhodamine B and 4-nitrophenol solutions with a stable poly-hydroxyl-iron/sepiolite catalyst. *Chemical Engineering Journal, 217*, 221–230. https://doi.org/10.1016/j.cej.2012.11.115

Grissa, R., Martinez, H., Cotte, S., Galipaud, J., Pecquenard, B., & Le Cras, F. (2017). Thorough XPS analyses on over-lithiated manganese spinel cycled around the 3V plateau. *Applied Surface Science, 411*, 449–456. https://doi.org/10.1016/j.apsusc.2017.03.205

Huang, Y., Lin, H., & Zhang, Y. (2020). Synthesis of MIL-101(Fe)/SiO_2 composites with improved catalytic activity for reduction of nitroaromatic compounds. *Journal of Solid State Chemistry, 283*, 121150. https://doi.org/10.1016/j.jssc.2019.121150

Imangaliyeva, A. N., Mastai, Y., & Seilkhanova, G. A. (2019). In situ synthesis and catalytic properties of Cu_2O nanoparticles based on clay materials and polyethylene glycol. *Journal of Nanoparticle Research, 21*, 1–11. https://doi.org/10.1007/s11051-019-4548-8

Jiang, D. B., Liu, X., Yuan, Y., Feng, L., Ji, J., Wang, J., Losic, D., Yao, H.-C., & Zhang, Y. X. (2020). Biotemplated top-down assembly of hybrid Ni nanoparticles/N doping carbon on diatomite for enhanced catalytic reduction of 4-nitrophenol. *Chemical Engineering Journal, 383*, 123156. https://doi.org/10.1016/j.cej.2019.123156

Kim, M., & Bae, S. (2018). Immobilization and characterization of Fe(0) catalyst on NaOH-treated coal fly ash for catalytic reduction of p-nitrophenol. *Chemosphere, 212*, 1020–1029. https://doi.org/10.1016/j.chemosphere.2018.09.006

Lin, C., Tao, K., Hua, D., Ma, Z., & Zhou, S. (2013). Size Effect of Gold Nanoparticles in Catalytic Reduction of p-Nitrophenol with $NaBH_4$. *Molecules, 18*(10), 12609–12620. https://doi.org/10.3390/molecules181012609

Liu, X., Ruiz, J., & Astruc, D. (2018). Compared Catalytic Efficiency of Click-Dendrimer-Stabilized Late Transition Metal Nanoparticles in 4-Nitrophenol Reduction. *Journal of Inorganic and Organometallic Polymers and Materials, 28*, 399–406. https://doi.org/10.1007/s10904-017-0666-x

Mandlimath, T. R., & Gopal, B. (2011). Catalytic activity of first row transition metal oxides in the conversion of p-nitrophenol to p-anninophenol. *Journal of Molecular Catalysis a: Chemical, 350*(1–2), 9–15. https://doi.org/10.1016/j.molcata.2011.08.009

Mejia, Y. R., & Reddy Bogireddy, N. K. (2022). Reduction of 4-nitrophenol using green-fabricated metal nanoparticles. *RSC Advances, 12*(29), 18661–18675. https://doi.org/10.1039/D2RA02663E

Menumerov, E., Hughes, R. A., & Neretina, S. (2016). Catalytic Reduction of 4-Nitrophenol: A Quantitative Assessment of the Role of Dissolved Oxygen in Determining the Induction Time. *Nano Letters, 16*(12), 7791–7797. https://doi.org/10.1021/acs.nanolett.6b03991

Miao, S., Shi, J., Sun, Y., Zhang, P., Shen, Z., Nian, H., Huang, J., Wang, X., & Zhang, P. (2018). Mineral abundances quantification to reveal the swelling property of the black cotton soil in Kenya. *Applied Clay Science, 161*, 524–532. https://doi.org/10.1016/j.clay.2018.02.003

Minz, S., Garg, S., & Gupta, R. (2018). Catalytic wet peroxide oxidation of 4-Nitrophenol over Al-Fe PILC: Kinetic study using Fermi's equation and mechanistic pathways based on TOC reduction. *Chemical Engineering Communications, 205*(5), 667–679. https://doi.org/10.1080/00986445.2017.1412310

Mohammadnezhad, G., & Ariaeinezhad, F. (2021). Synthesis of mesoporous flower-like iron oxide nanostructures from iron alkoxide precursor and their application in the catalytic reduction of 4-nitrophenol. *Journal of Porous Materials, 28*, 791–801. https://doi.org/10.1007/s10934-021-01034-y

Mu, B., Zhang, W., & Wang, A. (2014). Facile fabrication of superparamagnetic coaxial gold/halloysite nanotubes/Fe_3O_4 nanocomposites with excellent catalytic property for 4-nitrophenol reduction. *Journal of Materials Science, 49*, 7181–7191. https://doi.org/10.1007/s10853-014-8426-6

Park, J., & Bae, S. (2018). Formation of Fe nanoparticles on water-washed coal fly ash for enhanced reduction of p-nitrophenol. *Chemosphere, 202*, 733–741. https://doi.org/10.1016/j.chemosphere.2018.03.152

Park, J., Saratale, G. D., Cho, S.-K., & Bae, S. (2020). Synergistic effect of Cu loading on Fe sites of fly ash for enhanced catalytic reduction of nitrophenol. *Science of the Total Environment, 705*, 134544. https://doi.org/10.1016/j.scitotenv.2019.134544

Reijnders, L. (2006). Cleaner nanotechnology and hazard reduction of manufactured nanoparticles. *Journal of Cleaner Production, 14*(2), 124–133. https://doi.org/10.1016/j.jclepro.2005.03.018

Sensarma, S., Chakraborty, P., Banerjee, R., & Mukhopadhyay, S. (2016). Geochemical fractionation of Ni, Cu and Pb in the deep sea sediments from the Central Indian Ocean Basin: An insight into the mechanism of metal enrichment in sediment. *Geochemistry, 76*(1), 39–48. https://doi.org/10.1016/j.chemer.2015.10.002

Suwannarat, K., Thongthai, K., Ananta, S., & Srisombat, L. (2018). Synthesis of hollow trimetallic Ag/Au/Pd nanoparticles for reduction of 4-nitrophenol. *Colloids and Surfaces a: Physicochemical and Engineering Aspects, 540*, 73–80. https://doi.org/10.1016/j.colsurfa.2017.12.046

Tuo, Y., Liu, G., Dong, B., Yu, H., Zhou, J., Wang, J., & Jin, R. (2017). Microbial synthesis of bimetallic PdPt nanoparticles for catalytic reduction of 4-nitrophenol. *Environmental Science and Pollution Research, 24*, 5249–5258. https://doi.org/10.1007/s11356-016-8276-7

Ullah, N., Odda, A. H., Li, D., Wang, Q., & Wei, Q. (2019). One-pot green synthesis of gold nanoparticles and its supportive role in surface activation of non-woven fibers as heterogeneous catalyst. *Colloids and Surfaces a: Physicochemical and Engineering Aspects, 571*, 101–109. https://doi.org/10.1016/j.colsurfa.2019.03.076

Wan, D., Li, W., Wang, G., Chen, K., Lu, L., & Hu, Q. (2015). Adsorption and heterogeneous degradation of rhodamine B on the surface of magnetic bentonite material. *Applied Surface Science, 349*, 988–996. https://doi.org/10.1016/j.apsusc.2015.05.004

Wang, J., Zhang, Y., Ning, W., Zhang, P., Jin, B., Wang, Y., Zhang, W., Li, W., Wei, C., & Miao, S. (2021). Self-propelling nanomotor made from halloysite and catalysis in Fenton-like reaction. *Journal of the American Ceramic Society, 104*(9), 4867–4877. https://doi.org/10.1111/jace.17821

Ware, A., & Power, N. (2017). Modelling methane production kinetics of complex poultry slaughterhouse wastes using sigmoidal growth functions. *Renewable Energy, 104*, 50–59. https://doi.org/10.1016/j.renene.2016.11.045

Wu, G., Liang, X., Zhang, L., Tang, Z., Al-Mamun, M., Zhao, H., & Su, X. (2017). Fabrication of Highly Stable Metal Oxide Hollow Nanospheres and Their Catalytic Activity toward 4-Nitrophenol Reduction. *ACS Applied Materials & Interfaces, 9*(21), 18207–18214. https://doi.org/10.1021/acsami.7b03120

Wunder, S., Polzer, F., Lu, Y., Mei, Y., & Ballauff, M. (2010). Kinetic Analysis of Catalytic Reduction of 4-Nitrophenol by Metallic Nanoparticles Immobilized in Spherical Polyelectrolyte Brushes. *Journal of Physical Chemistry C, 114*(19), 8814–8820. https://doi.org/10.1021/jp101125j

Xiong, Z., Zhang, H., Zhang, W., Lai, B., & Yao, G. (2019). Removal of nitrophenols and their derivatives by chemical redox: A review. *Chemical Engineering Journal, 359*, 13–31. https://doi.org/10.1016/j.cej.2018.11.111

Yan, N., Zhao, Z., Li, Y., Wang, F., Zhong, H., & Chen, Q. (2014). Synthesis of Novel Two-Phase Co@SiO_2 Nanorattles with High Catalytic Activity. *Inorganic Chemistry, 53*(17), 9073–9079. https://doi.org/10.1021/ic501092k

Yan, F., Hu, Z., Tian, Q., & Wang, B. (2020). Facile synthesis of porous hollow Au nanoshells with enhanced catalytic properties towards reduction of p-nitrophenol. *Inorganic Chemistry Communications, 116*, 107896. https://doi.org/10.1016/j.inoche.2020.107896

Yang, Y., Zeng, D., Shao, S., Hao, S., Zhu, G., & Liu, B. (2019). Construction of core-shell mesoporous carbon nanofiber@nickel cobaltite nanostructures as highly efficient catalysts towards 4-nitrophenol reduction. *Journal of Colloid and Interface Science, 538*, 377–386. https://doi.org/10.1016/j.jcis.2018.12.003

Zermane, F., Bouras, O., Baudu, M., & Basly, J. P. (2010). Cooperative coadsorption of 4-nitrophenol and basic yellow 28 dye onto an iron organo-inorgano pillared montmorillonite clay. *Journal of Colloid and Interface Science, 350*(1), 315–319. https://doi.org/10.1016/j.jcis.2010.06.040

Zhang, G., Gao, Y., Zhang, Y., & Guo, Y. (2010). Fe_2O_3-Pillared Rectorite as an Efficient and Stable Fenton-Like Heterogeneous Catalyst for Photodegradation of Organic Contaminants. *Environmental Science & Technology, 44*(16), 6384–6389. https://doi.org/10.1021/es1011093

Zhang, P., Sun, X., Guo, J., Wang, Y., Zhang, W., Ning, W., Li, W., Wei, C., Shi, X., & Miao, S. (2022). Deep-sea clays using as active Fenton catalysts for self-propelled motors. *Journal of the American Ceramic Society, 105*(6), 3797–3808. https://doi.org/10.1111/jace.18348

Zhao, P., Feng, X., Huang, D., Yang, G., & Astruc, D. (2015). Basic concepts and recent advances in nitrophenol reduction by gold- and other transition metal nanoparticles. *Coordination Chemistry Reviews, 287*, 114–136. https://doi.org/10.1016/j.ccr.2015.01.002

Zwietering, M. H., Jongenburger, I., Rombouts, F. M., & van 't Riet, K. (1990). Modeling of the bacterial growth curve. *Applied and Environmental Microbiology, 56*(6), 1875–1881. https://doi.org/10.1128/aem.56.6.1875-1881.1990